Locally optimal geometry for surface-enhanced diffusion

Christensen, Anneline H.; Gupta, Ankur; Chen, Guang; Peters, Winfried S.; Knoblauch, Michael; Stone, Howard A.; Jensen, Kaare H.

Link back to DTU Orbit

Locally optimal geometry for surface-enhanced diffusion

Anneline H. Christensen [ORCID],[1] Ankur Gupta [ORCID],[2] Guang Chen,[3] Winfried S. Peters [ORCID],[4] Michael Knoblauch,[4] Howard A. Stone [ORCID],[5] and Kaare H. Jensen [ORCID][1,*]

[1]*Department of Physics, Technical University of Denmark, DK-2800 Kgs. Lyngby, Denmark*
[2]*Department of Chemical and Biological Engineering, University of Colorado, Boulder, Colorado 80309, USA*
[3]*Department of Advanced Manufacturing and Robotics, College of Engineering,*
Peking University, Beijing 100871, People's Republic of China
[4]*School of Biological Sciences, Washington State University, Pullman, Washington 99164, USA*
[5]*Department of Mechanical and Aerospace Engineering, Princeton University, Princeton, New Jersey 08544, USA*

Molecular diffusion in bulk liquids proceeds according to Fick's law, which stipulates that the particle current is proportional to the conductive area. This constrains the efficiency of filtration systems in which both selectivity and permeability are valued. Previous studies have demonstrated that interactions between the diffusing species and solid boundaries can enhance or reduce particle transport relative to bulk conditions. However, only cases that preserve the monotonic relationship between particle current and conductive area are known. In this paper, we expose a system in which the diffusive current increases when the conductive area diminishes. These examples are based on the century-old theory of a charged particle interacting with an electrical double layer. This surprising discovery could improve the efficiency of filtration and may advance our understanding of biological pore structures.

I. INTRODUCTION

Molecular diffusion across micro- and nanoporous structures occurs in numerous industrial and biological processes, such as filtering of air- or water-borne particles [1], separation of chemical and biological agents [2], and salinity gradient nanopore energy harvesting [3,4]. It is also critical for the transport of nutrients and signaling molecules (and pathogens) between biological cells [5–9]. The principal consequence of Fick's first law of diffusion is that the particle current $I \propto \sigma_0$ scales monotonically with the conductive area σ_0. Combining the antagonistic criteria of permeability (which favors a large pore aperture) and selectivity (requiring small pores) thus appears out of reach. In this paper, we propose that a charged membrane can circumvent these constraints.

Chemical separation processes are responsible for more than 10% of the worlds energy consumption [2]. Membrane separation offers the advantage of low energy operating cost and is thus a green and economical alternative to traditional processes, such as distillation. However, membranes have a high initial capital expense, and increasing the total membrane area (or the pore density) may not always be feasible due to space and cost constraints. Therefore, maximizing the transport capacity of individual pores is an essential and widely recognized problem in filtration physics [10]. This, however, is hard because small pores generally permit smaller diffusive current.

It is well-established that particle-surface forces can enhance or reduce the total diffusion current relative to Fick's law [11], via, e.g., electrostatic interactions [11–17], chemical adsorption and hydrodynamic hindrance [18–22], pore geometry [6,23], or, for instance, Taylor-Aris dispersion [24,25]. The *monotonic relationship* between particle current I and the pore area σ_0, however, is preserved in all cases reported thus far.

The link between tracer particle motion and the pore energy landscape may nevertheless hold clues to cases that break the area monotonicity. First, according to the Boltzmann principle, the equilibrium concentration of tracer particles is influenced by the energy landscape due to, e.g., van der Waals and electrostatic potentials, which can be attractive or repulsive, depending on charge [26]. Second, the link between the pore shape, size, and topology and the energy landscape is nonlinear [12,13].

In this paper, we develop a theory that links the energy landscape in the pore and the diffusive current, consistent with the experimental data from [12,13]. Surprisingly we find that for even very simple interactions (e.g., an electrical double layer), violations of Ficks law occur in a significant part of the parameter space. We introduce the diffusion cross-section σ as the effective pore area experienced by a tracer particle. This quantity is analogous to the nuclear cross-section where the scattering probability depends on geometry and interactions [27]. For particles traversing slender pores, we show that in certain cases, the diffusion cross-section depends nonmonotonically on the geometric pore area σ_0. As an example, we consider a charged particle interacting with an electrical double layer formed between two charged parallel plates. We provide analytical formulas characterizing the relationship between pore geometry and interaction strength, and the diffusion cross-section. Results are then extended to other conduit geometries. Finally, we show that concentric channels

---

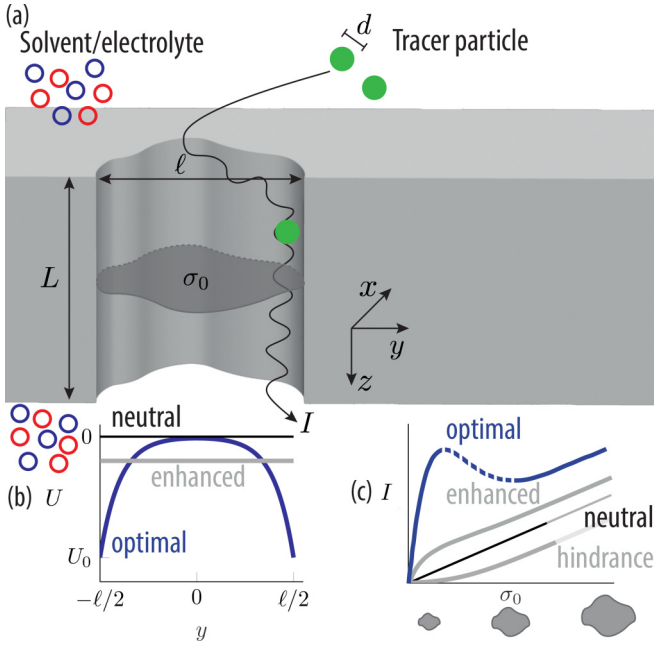*Corresponding author: khjensen@fysik.dtu.dk

FIG. 1. Surface-enhanced diffusion. (a) A concentration difference Δc of tracer particles (green dots, diameter d) leads to a diffusive current I across a slender channel of length L and uniform cross-sectional area $\sigma_0 \sim \ell^2$. (b) Tracer particles interact with the channel boundaries through an energy potential U. (c) Surface interactions impact the diffusive current I and can either reduce or enhance transport. We demonstrate an optimal case in which the current grows as the geometric pore area diminishes (marked by the dashed blue line).

offer the optimal tradeoff between permeability and selectivity when compared to circular and slit pores of equal area.

II. RESULTS

We consider diffusive transport of *tracer* particles (diameter d) between two reservoirs connected by a slender cylindrical channel of length L and uniform cross-sectional area σ_0 (Fig. 1). The tracer particle concentration c is small compared to all other constituents of the solution, such as the solvent, electrolytes, and dissolved gases. Our objective is to explore conditions that maximize the tracer particle current I between the two reservoirs while preventing larger molecules or contaminants from migrating between the two regions. The pore selectivity is determined by the diameter ℓ of the largest spherical particle able to enter the channel (Fig. 1). The simplest approach is to match the pore and particle size, i.e., $\ell = d$. However, because the current I scales with the geometric pore area ($\sigma_0 \sim \ell^2$ for a circular channel), obtaining high selectivity in this manner is generally associated with reduced permeability.

To move beyond the direct relationship between particle current I and pore area σ_0, we consider the general case of interactions between a tracer particle and the energy landscape U induced by the presence of channel boundaries (Fig. 1). We assume that the energy landscape $U(x, y)$ and the pore cross-section shape and area σ_0 are invariant along the main channel axis z. The flux of tracer particles can be described

using the Nernst-Planck equation, and we assume that molecular diffusion is the dominant transport mechanism (Appendix 6). Given a difference in concentration Δc across the pore, the diffusive flux $\mathbf{J}$ follows Fick's law $\mathbf{J} = -D\nabla c$, where D is the molecular diffusion coefficient. The particle current I along the main z axis of the channel can be determined by integration over the pore cross-section

$$I = \int_{\sigma_0} \mathbf{J} \cdot \mathbf{e}_z \, dA = -\int_{\sigma_0} D\nabla c \cdot \mathbf{e}_z \, dA, \quad (1)$$

where $\mathbf{e}_z$ is a unit vector normal to the pore (x, y) plane. In the absence of particle-surface interactions ($U = 0$), the particle distribution is uniform in the transverse (x, y) plane and the steady-state concentration $c(x, y, z) = c_0(z) = \Delta c(L - z)/L$ only depends on the axial position z. This leads to the familiar Ohmic formulation of Fick's law [28] $I_* = \sigma_0 D\Delta c/L$, where the current I_* increases linearly with the concentration difference Δc, the geometric area of the pore σ_0, and the diffusion constant D but decays inversely with the channel length L.

If, however, energy can be gained by particles residing in the pore ($U < 0$), then we expect the concentration $c > c_0$ of tracer particles to exceed the neutral case because they are attracted by the boundaries. To compute the precise magnitude of this effect on the current law in Eq. (1), we presume the tracer particles are in thermal equilibrium such that their concentration c follows the Boltzmann distribution

$$c(x, y, z) = c_0(z)e^{-U(x,y)/(k_BT)}, \quad (2)$$

where c_0 is the interaction-free concentration ($U = 0$), k_B is the Boltzmann constant, and T is temperature [29,30]. Finally, we can express the current [Eq. (1)] as

$$I = \sigma D\frac{\Delta c}{L}, \quad \text{where} \quad \sigma = \int_{\sigma_0} e^{-U(x,y)/(k_BT)} \, dA, \quad (3)$$

is the diffusion cross-section that differs from the geometric area (σ_0) depending on the sign, magnitude, and spatial variation of the potential U.

At this point, it is important to reiterate that our objective is to optimize the pore geometry for both selectivity and permeability. In other words, we seek to maximize the diffusion cross-section σ while minimizing the geometric area σ_0 (or selectivity length ℓ). Although these opposing criteria appear fundamentally incompatible, an intriguing possibility is the existence of one or more extrema in the diffusion cross-section, corresponding to

$$\frac{d\sigma}{d\ell} = 0. \quad (4)$$

Our primary goal is identifying a local maximum in the diffusion cross-section $\sigma \propto I$ based on Eqs. (3) and (4). (Global extrema are physically impossible because the effects of surface-interactions are negligible in macroscopic pores.)

In the following, we provide an example confirming the existence of solutions to Eq. (4) based on the well-established theory of a charged particle interacting with an electrical double layer. To highlight the main physical effects, we restrict our attention to transport along the z axis between two parallel plates of width w held a variable distance $2h = \ell$ apart [Fig. 2(a)]. (Results applicable to circular and concentric
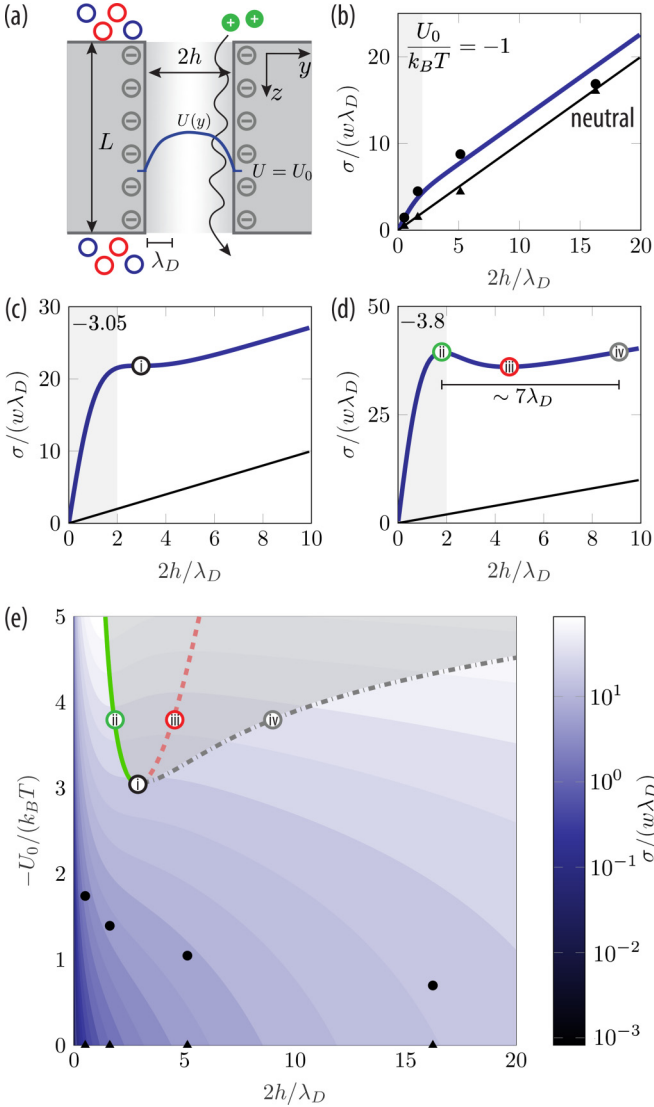
FIG. 2. Surface-enhanced diffusion in a slit. (a) A positively charged tracer particle (green) diffuses along a pore with negatively charged boundaries. The presence of an electrolyte induces the energy potential $U(y)$; see Eq. (5). (b)–(d) Diffusion cross-section $\sigma/(w\lambda_D)$ plotted as function of the channel height $2h/\lambda_D$ for energies $U_0/(k_BT) = \{-1, -3.05, -3.8\}$ [Eq. (6)]. The thin solid line corresponds to the interaction-free $\sigma = \sigma_0$ case. At low energies (b), the diffusion cross-section exceeds the geometric area $\sigma > \sigma_0$ and increases monotonically with channel height $2h$. However, near the energy $U_0/(k_BT) = -3.05$, a saddle point (i) appears where the current $I \sim \sigma$ is approximately independent of channel height in the range $2 < 2h/\lambda_D < 5$. (d) Remarkably, for stronger interactions [e.g., $U_0/(k_BT) = -3.8$], local extrema (ii and iii) in the diffusion cross-section appear. (e) Contour plot of the diffusion cross-section $\sigma/(w\lambda_D)$ as function of energy $U_0/(k_BT)$ and relative channel height $2h/\lambda_D$. Experimental data from Ref. [12] [points in panels (b) and (e)] are not inconsistent with theory.

pores, as well as dipolar molecules are discussed below and in Figs. 3 and 6. See also Appendices 1 and 2.)

Proceeding with our treatment of the slit geometry we consider a tracer particle interacting with an electric double layer. This ubiquitous structure appears near charged surfaces
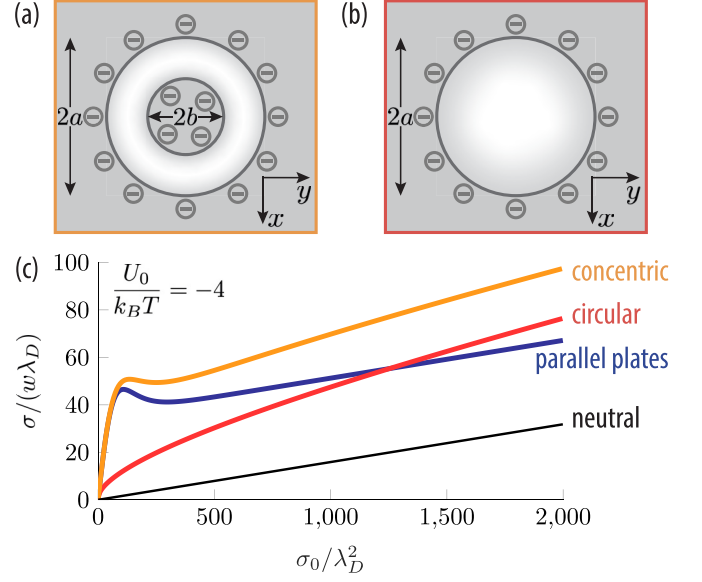

FIG. 3. Comparison of diffusion cross-sections. (a) Top-view of a concentric geometry with outer radius a, constant inner radius $b = 10\lambda_D$ and geometric cross-sectional area $\sigma_0 = \pi(a^2 - b^2)$. (b) Top-view of a circular geometry with radius a and $\sigma_0 = \pi a^2$. All boundaries are charged with surface potential ζ. (c) Diffusion cross-sections $\sigma/(w\lambda_D)$ plotted as functions of the geometric cross-sectional area σ_0/λ_D^2 for energy $U_0/(k_BT) = -4$. Blue (parallel plates), orange (concentric), and red (circular). The width of the parallel plates is chosen as $w = 2\pi b$ to match the circumference of the inner concentric cylinder.

exposed to an electrolyte solution containing, for instance, salts such as NaCl or KCl. Because the surface is charged (electrical potential ζ), the electrolyte ions in the solvent form a boundary layer near the interface. For a tracer particle of charge q, the equilibrium distribution of electrolyte ions approximately corresponds to the interaction energy (Appendix 5),

$$U(y) = U_0 \frac{\cosh(y/\lambda_D)}{\cosh(h/\lambda_D)}, \tag{5}$$

where $U_0 = \zeta q$ is proportional to the tracer particle charge q and the surface potential ζ. The parameter $\lambda_D = \sqrt{\varepsilon k_B T/(2c_{\mathrm{el}}(Z_{\mathrm{el}}e)^2)}$ is the Debye length that describes the range of the electrical force from the channel surface on the tracer particle [31]. Here, ε is the permittivity, e the elementary charge, and Z_{el} and c_{el}, respectively, the valence and concentration of the ions in the bulk electrolyte solution.

The charge of tracer particles considered here varies from $|q| \sim (1-3)e$ for water soluble ions to $|q| > 10e$ for some charged proteins (e.g., supercharged GFP [32]). Typical surface potentials are of the order $|\zeta| \approx 10$–100 mV for, e.g., silicon [33] and plasma membranes of biological cells [34]. The interaction energy of a tracer particle thus falls in the range $|U_0/(k_BT)| \sim 2$–20 for $|\zeta| = 50$ mV and $|q| = (1-10)e$ at room temperature ($T = 300$ K).

Having established the basic components of the double-layer problem, we can evaluate the diffusion cross-section [Eq. (3)], given in the slit geometry by

$\sigma = 2w \int_0^h \exp[-U(y)/(k_B T)]\,dy$ where U is defined in Eq. (5). For weak interactions, we recover the geometric cross-section, i.e., $\sigma = 2hw = \sigma_0$. For stronger interactions, however, two behaviors are anticipated: when the double layers overlap $2h \ll \lambda_D$ the energy $U \approx U_0$ is approximately constant, and the integral yields $\sigma = \sigma_0 \exp[-U_0/(k_B T)]$. In contrast, when $2h \gg \lambda_D$, molecules in the bulk are unaffected by the wall interactions, and the integral only deviates from unity inside the double layers. In this limit, we thus expect the diffusion cross-section to scale linearly with the geometric area but with an offset due to the (small but finite) wall interactions: $\sigma \approx \sigma_0 + 2w\lambda_D \exp[-U_0/(k_B T)]$.

The transition between the two geometric cases occurs when h is of order λ_D, and is not necessarily monotonic, because of the nonlinear functional relationship in the integral. To further unpack these effects, we compute the cross-section σ directly from Eq. (5)

$$\sigma = 2wh\left[I_0\left(-\frac{U_0}{k_B T}\frac{1}{\cosh(h/\lambda_D)}\right)\right.$$
$$\left. + \frac{\lambda_D}{h}\sum_{k=1}^{\infty}\frac{2}{k}I_k\left(-\frac{U_0}{k_B T}\frac{1}{\cosh(h/\lambda_D)}\right)\sinh\left(\frac{kh}{\lambda_D}\right)\right], \quad (6)$$

where I_k is the modified Bessel function of the first kind of order k and we have used the identities $\cosh(x) = \cos(ix)$, $\sinh(x) = -i\sin(ix)$, and $\exp(p\cos(u)) = I_0(p) + 2\sum_{k=1}^{\infty}I_k(p)\cos(ku)$.

We will now discuss the basic properties of the surface-enhanced diffusion cross-section σ [Eq. (6)]. First, we note that it reduces to the geometric pore area $\sigma = 2hw = \sigma_0$ in the limit of negligible energy $|U_0/(k_B T)| \ll 1$. For energies of order unity $-U_0/(k_B T) \sim 1$, Eq. (6) stipulates that the diffusion area σ is a few times larger than the geometric pore area for reasonably small pores, that is when $2h/\lambda_D < 5$. Both predictions are in accord with experimental data from Ref. [12] [Fig. 2(b)], which studied diffusion of fluorescein, rhodamine B, and rhodamine 6G in nanochannels of relative heights $2h/\lambda_D = 0.5$–167. The molecular and surface properties in these experiments correspond to interaction energies in the range $-U_0/(k_B T) \approx 0$–2. Note that in Fig. 2 the diffusion cross-section σ is normalized by the double layer area $w\lambda_D$ to show how σ, and thus the diffusive current [Eq. (3)], changes as h is varied.

At energies beyond the experimentally justified foundation, Eq. (6) predicts several surprising features of the diffusion cross-section σ as function of the channel height $2h/\lambda_D$ and energy $U_0/(k_B T)$ [Figs. 2(c) and 2(d)]: Strikingly, when the energy exceeds $-U_0/(k_B T) \approx 3$, the cross-section deviates from monotonicity. A saddle point appears when the channel height $2h/\lambda_D \sim 2.8$ [Fig. 2(c)]. Beyond this point, two distinct branches appear corresponding to two extrema. The peak diffusion area occurs because the interaction energy U [Eq. (5)] diminishes faster with channel height $2h$ than the surface integral grows with the plate-to-plate distance $2h$. (Note that varying λ_D while keeping the channel height $2h$ constant, however, does not give rise to a nonmonotonic behavior in the diffusion cross-section σ as seen in Fig. 2, as both axes are inversely proportional to λ_D.)

To highlight the significance of the optimum, we consider the energy $U_0/(k_B T) = -3.8$ [Fig. 2(d)]. Here, the peak transport occurs at $2h/\lambda_D \simeq 1.8$. The transport rate in this geometry is equal to the particle current through an approximately five times larger channel ($2h/\lambda_D \simeq 9$). The selectivity in the smaller pore has thus increased fivefold with no impact on permeability. Inspection of the surface plot [Fig. 2(e)] reveals a large region of the parameters space in which the diffusion cross-section either increases or remains stationary, as the geometric area of the pore decreases. The peak diffusion area occurs around when the electric double layers start to overlap. For both strongly overlapping and nonoverlapping double layers, the diffusion cross-section increases linearly with channel height $2h$. For strongly overlapping double layers, $2h/\lambda_D \ll 1$, the potential is approximately constant across the channel and $\sigma \simeq 2hwe^{-\frac{U_0}{k_B T}}$, while for strongly nonoverlapping double layers, $2h/\lambda_D \gg 1$, the diffusion cross-section increases as $2hw$, but with an offset (see Appendix 3).

The scaling analysis above also holds for particles carrying charges of the same sign as the pore wall, $U_0/(k_B T) > 0$. In this case Eq. (6) predicts the transport rate to be monotonically increasing with pore area, but reduced compared to the neutral case, regardless of the absolute value of the energy scale $U_0/(k_B T)$.

We emphasize that though Eq. (5) and the cases shown in Fig. 2 are based on a linearization of the Poisson-Boltzmann equation, they can still be valid for large interaction energies $|U_0/(k_B T)| > 1$. By considering the coupled problem, we see that the dilute tracer particles' contribution to the charge distribution in the electrical double layer is negligible when the quantity $\frac{c_0}{c_{\rm el}}\frac{Z^2}{Z_{\rm el}^2}$ is relatively small (see Appendix 6). We can therefore use the linearized Poisson-Boltzmann equation to find the electric potential in the channel when the electrolyte-wall interactions are weak (i.e., for $|Z_{\rm el}e\zeta/(k_B T)| < 1$), while still allowing the interaction energy, U_0, which depends on the tracer particle valence, Z, as well, to be large.

Further, we note that if we move beyond the validity of the linearized Poisson-Boltzmann equation, we can find the diffusion cross-section numerically using the full Poisson-Boltzmann equation, which, depending on the choice of tracer particle valence Z and surface potential ζ, may differ slightly from the linearized solution. The nonmonotonic effect is generally not, however, substantially reduced (see Appendix 5).

Up to this point we have restricted our attention to the parallel plate geometry. Expanding our analysis to concentric and circular geometries confirms the general physical picture discussed above (Fig. 3). Unsurprisingly, transport in a shallow concentric channel [Figs. 3(a) and 3(c)] closely follows the preceding analysis due to the geometric similarity. However, no optimal double layer geometry exists in a circular pore [Figs. 3(b) and 3(c)]. The phenomenon is absent because the length of the electric double layer (which scales with the circumference) increases faster than the boundary layer effect diminishes with pore diameter (Appendix 1). A detailed comparison of the three pore geometries [Fig. 3(c)] reveals that while they are all superior to the neutral case, a concentric pore is generally the most favorable geometry for surface-enhanced diffusion. Its strong performance relative to

a slit of equal area is due to the larger perimeter and thus larger electric double-layer.

Extending the analysis to dipolar molecules, such as certain proteins, or other energy landscapes is straightforward. Our theory is not inconsistent with data from neutral molecules (Appendix 2). Moreover, we show in Appendix 4 that neither pure multipolar interactions, nor potentials of the form $U = U_0 f(y/\ell)$, where f is a nondimensional function, can lead to optima.

III. CONCLUSION

We have demonstrated the feasibility of transport beyond the monotonic area dependence of diffusive transport across small pores reported previously. This suggests potential improvements to existing filtration technology in terms of both throughput, energy consumption, and selectivity. It may also aid in the understanding of biological pore structures, such as pili that temporarily connect bacterial cells [9] and consist of proteins exhibiting complex patterns of surface charges [35], or plasmodesmata in plant cells that show a concentric structure [8]. Our predictions are based on robust electrostatic effects that are consistent with data in the low-energy limit. We anticipate that our results will stimulate experimentalists to explore the potentially impactful high-energy regime which, we acknowledge, still awaits experimental validation.

ACKNOWLEDGMENTS

APPENDIX

1. Cylindrical geometries

In this Appendix we find the diffusion cross-section, σ, for cylindrical pores with circular and concentric geometries. We start by considering a cylindrical pore with a circular cross-sectional area with radius a [Fig. 4(a)]. The diffusion cross-section [Eq. (3)] is

$$\sigma = 2\pi \int_0^a e^{-U(r)/(k_B T)} r\,dr, \qquad (A1a)$$

where r is the radial coordinate. For the example of a charged tracer particle interacting with an electrical double layer, the interaction energy $U = q\psi$ is approximately

$$U(r) = U_0 \frac{I_0(r/\lambda_D)}{I_0(a/\lambda_D)}, \qquad (A1b)$$

where I_0 is the modified Bessel function of the first kind of order zero. Here, the electric potential in the channel, ψ, is found using the linearized Poisson-Boltzmann equation in cylindrical coordinates [36],

$$\frac{\partial^2 \psi}{\partial r^2} + \frac{1}{r}\frac{\partial \psi}{\partial r} = \frac{1}{\lambda_D^2}\psi, \qquad (A1c)$$
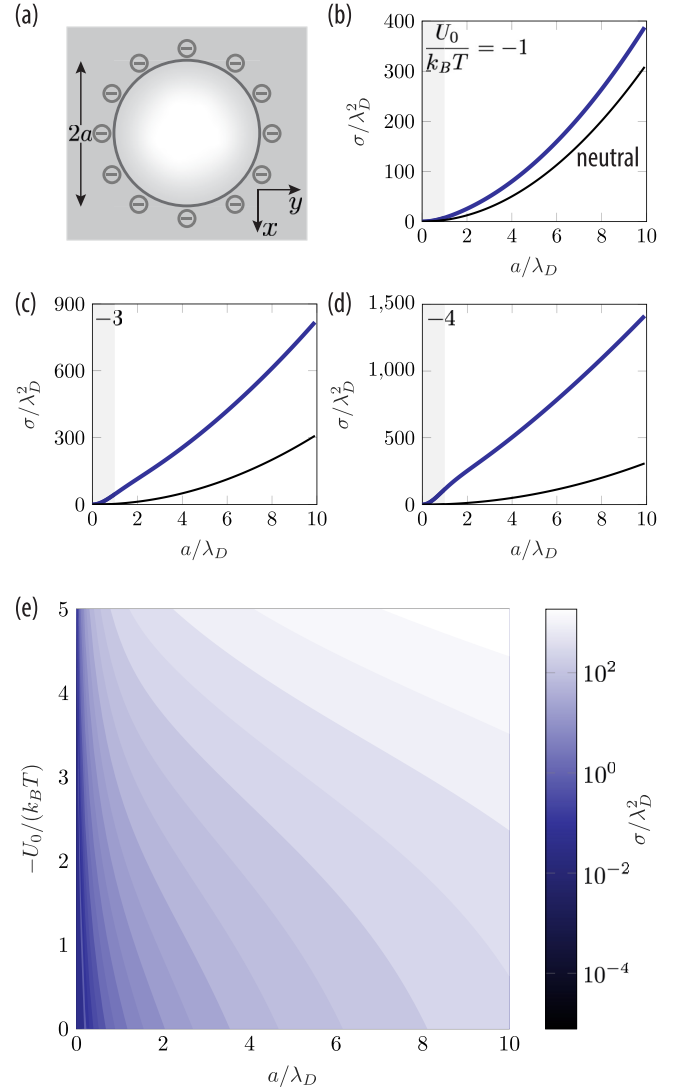

FIG. 4. Surface-enhanced diffusion in a circular geometry. (a) Top-view of circular channel with radius a and surface potential ζ. (b)–(d) Diffusion cross-section normalized by the Debye length squared σ/λ_D^2 plotted as a function of the channel radius a/λ_D for energies $U_0/(k_B T) = \{-1, -3, -4\}$ [Eq. (A1a)]. The thin solid line corresponds to the interaction-free case $\sigma = \sigma_0 = \pi a^2$. The diffusion cross-section exceeds the geometric area $\sigma > \sigma_0$ but increases monotonically with channel radius a. (e) Contour plot of the diffusion cross-section σ/λ_D^2 as function of energy $U_0/(k_B T)$ and relative channel radius a/λ_D.

when the channel boundary is charged with surface potential ζ, i.e., with $\psi(r = a) = \zeta$.

The diffusion cross-section, σ, increases monotonically with increasing pore radius a [Figs. 4(b)–4(e)], and is greater than the diffusion cross-section in the interaction-free case ($\sigma = \sigma_0 = \pi a^2$) when $U_0/(k_B T) < 1$.

Next, we consider a cylindrical pore with a concentric cross-sectional area with outer radius a and inner radius b [Fig. 5(a)]. The diffusion cross-section [Eq. (3)] is

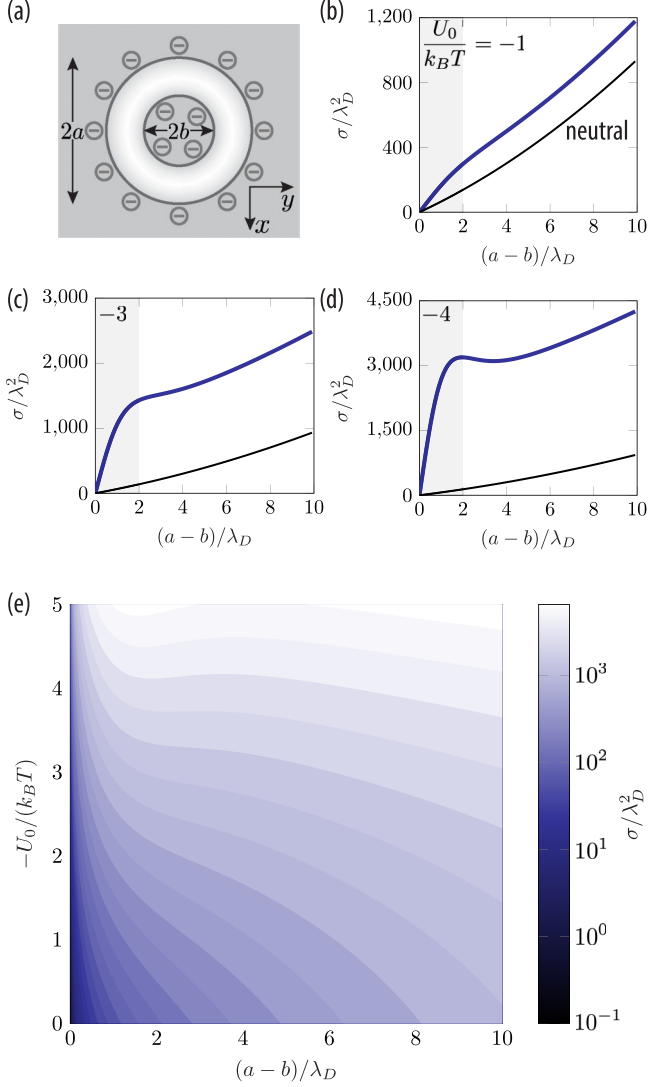$$\sigma = 2\pi \int_b^a e^{-U(r)/(k_B T)} r\,dr. \qquad (A2a)$$

FIG. 5. Surface-enhanced diffusion in a concentric geometry. (a) Top-view of concentric circular channel with outer radius a and inner radius b. Transport occurs in the gap between the two cylinders. Both surfaces are charged with surface potential ζ. (b)–(d) Diffusion cross-section normalized by the Debye length squared σ/λ_D^2 plotted as a function of the channel gap $(a-b)/\lambda_D$ for energies $U_0/(k_BT) = \{-1, -3, -4\}$ [Eq. (A2a)]. The inner radius is kept constant $b = 10\lambda_D$. The thin solid line corresponds to the interaction-free case $\sigma = \sigma_0 = \pi(a^2 - b^2)$. The diffusion cross-section exceeds the geometric area $\sigma > \sigma_0$ but increases monotonically with channel gap $(a-b)/\lambda_D$ at low energies (b). (d) For stronger interactions (e.g., $U_0/(k_BT) = -4$), a local maximum in the diffusion cross-section appears. (e) Contour plot of the diffusion cross-section σ/λ_D^2 as function of energy $U_0/(k_BT)$ and relative channel opening $(a-b)/\lambda_D$.

For the example of a tracer particle with charge q interacting with an electrical double layer, the interaction energy $U = q\psi$ is approximately

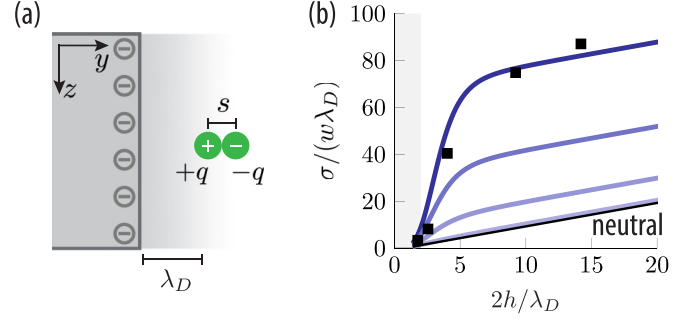$$U(r) = U_0[k_1 I_0(r/\lambda_D) + k_2 K_0(r/\lambda_D)], \quad \text{(A2b)}$$

FIG. 6. Dipole interactions. (a) Diagram of an electric dipole (separation distance s and charge q) near a charged wall in an electrolyte solution. The dipole is oriented with the positive charge closest to the negatively charged wall. (b) Enhanced diffusion cross-section for a dipole with $s = 0.68\lambda_D$ and $U_0/(k_BT) = \{-1, -5, -8, -10\}$ (bottom to top). The thin black line is the geometric cross-sectional area $\sigma_0 = 2w(h - s/2)$ and the black squares are experimental data from Ref. [13] on aspirin.

with constants

$$k_1 = \frac{K_0(b/\lambda_D) - K_0(a/\lambda_D)}{K_0(b/\lambda_D)I_0(a/\lambda_D) - I_0(b/\lambda_D)K_0(a/\lambda_D)}, \quad \text{(A2c)}$$

$$k_2 = \frac{I_0(a/\lambda_D) - I_0(b/\lambda_D)}{K_0(b/\lambda_D)I_0(a/\lambda_D) - I_0(b/\lambda_D)K_0(a/\lambda_D)}, \quad \text{(A2d)}$$

where K_0 is the modified Bessel function of the second kind of order zero. Here, the electric potential is again found using the linearized Poisson-Boltzmann equation in cylindrical coordinates [Eq. (A1c)]. This time the potential between the two cylinders is found assuming both the inner and outer cylinders are charged with surface potential ζ, i.e., Eq. (A1c) is solved with boundary conditions $\psi(r = a) = \psi(r = b) = \zeta$. Figures 5(b)–5(d) show the diffusion cross-section as a function of the gap between the two cylinders $(a-b)/\lambda_D$ for different energy scales $U_0/(k_BT)$ for a constant inner radius $b = 10\lambda_D$. The gap between the inner and outer cylinder is then varied by varying the outer radius a. As is the case for the parallel plate geometry (Fig. 2) the diffusion cross-section in a concentric geometry also shows a nonmonotonic behaviour for stronger interactions [e.g., for $U_0/(k_BT) = -4$, Figs. 5(d) and 5(e)].

2. Dipolar tracer particles

In the preceding analysis, we have focused exclusively on charged particles. In this Appendix, however, we look at how the transport of neutral, but polar molecules, are affected by surface interactions in an electrical double layer. Transport of neutral polar molecules, such as certain proteins, is widespread in both nature and technology. To elucidate how such molecules are influenced by surface interactions, we extend our parallel-plate theory to include dipolar molecules (Fig. 6).

The energy of a molecule comprising two charges $\pm q$ separated by a distance s in an electrical double layer is approximately

$$U_{\text{DP}}(y) = U_0 \frac{s}{\lambda_D} \frac{\sinh(y/\lambda_D)}{\cosh(h/\lambda_D)}, \quad \text{(A3)}$$

in the parallel plate geometry with the plates placed a distance $2h$ apart. Here, the interaction energy is found from $U_{DP} = -\mathbf{p} \cdot \mathbf{E}$, where $\mathbf{p} = q\mathbf{s}$ is the dipole moment, with $\mathbf{s}$ the separation distance, $s = |\mathbf{s}|$, and $\mathbf{E} = -\nabla\psi$ is the electric field in the channel [37]. ψ is the electric potential in the channel, here found using the linearized Poisson-Boltzmann equation assuming both channel walls are charged with surface potential ζ. Further, we assume that, say, the positively charged side of the dipoles is always oriented towards the nearest negatively charged surface.

We then find the diffusion cross-section [Eq. (3)] as

$$\sigma_{DP} = 2w \int_0^{h-s/2} e^{-U_{DP}(y)/(k_B T)} dy, \tag{A4}$$

where the limits in the integral take into account the positions available to the center of the dipole. Using Eqs. (A4) and (A3) the diffusion cross-section for the dipolar case in the parallel plate geometry is

$$\sigma_{DP} = w\lambda_D \left\{ \frac{2h-s}{\lambda_D} J_0 \left[\frac{s}{\lambda_D} \frac{U_0}{k_B T} \frac{1}{\cosh(h/\lambda_D)} \right] \right.$$

$$+ 2 \sum_{k=1}^{\infty} \frac{1}{k} J_{2k} \left[\frac{s}{\lambda_D} \frac{U_0}{k_B T} \frac{1}{\cosh(h/\lambda_D)} \right] \sinh\left[\frac{k(2h-s)}{\lambda_D} \right]$$

$$- 8 \sum_{k=1}^{\infty} \frac{1}{2k-1} J_{2k-1} \left[\frac{s}{\lambda_D} \frac{U_0}{k_B T} \frac{1}{\cosh(h/\lambda_D)} \right]$$

$$\left. \times \sinh^2\left[\frac{(2k-1)(2h-s)}{4\lambda_D} \right] \right\}, \tag{A5}$$

where J_k is the Bessel function of the first kind of order k. To obtain Eq. (A5) we have also made use of the following identities:

$$\cosh(x) = \cos(ix),$$

$$\sinh(x) = -i\sin(ix),$$

$$2\sinh^2(x) = \cosh(2x) - 1,$$

$$\sin(x) = \cos(x - \pi/2),$$

$$e^{p\cos u} = I_0(p) + 2\sum_{k=1}^{\infty} I_k(p)\cos(ku),$$

$$I_k(u) = i^{-k} J_k(iu),$$

$$i^k \sin\left(ikx - \frac{k\pi}{2} \right) = \begin{cases} -i\cos(ikx) & \text{if } k \text{ is odd} \\ \sin(ikx) & \text{if } k \text{ is even} \end{cases},$$

and

$$-i^k \sin\left(\frac{k\pi}{2} \right) = \begin{cases} -i & \text{if } k \text{ is odd} \\ 0 & \text{if } k \text{ is even} \end{cases}.$$

The resultant diffusion cross-section σ_{DP} is not qualitatively inconsistent with experimental data [Fig. 6(b)]. In contrast to diffusion of charged particles [Eq. (6), Fig. 2], however, no optimal channel size exists for dipolar molecules.

3. Nonoverlapping electrical double layers

In the following Appendix we find the diffusion cross-section for a charged tracer particle interacting with an electrical double layer in the limit of strongly nonoverlapping electrical double layers. We start by considering the parallel plate geometry with the plates placed a distance $2h$ apart and in the limit $2h/\lambda_D \gg 1$. Later we extend the theory to also include channels with a circular cross-section.

When the two charged pore walls are far away from each other, i.e., when $2h/\lambda_D \gg 1$, we find that the diffusion cross-section is on the form

$$\sigma = \sigma_0 + w\Delta h, \tag{A6}$$

where $\sigma_0 = 2hw$ is the geometric cross-section, w is the width of the channel and Δh is an offset. Equation (A6) is found from Eq. (3) by letting the electric potential in the interaction energy $U = q\psi$ be the electric potential from a single wall. When the charged pore walls are far from each other, $2h/\lambda_D \gg 1$, the electric potentials from each wall do not interact, and we can approximate the potential in the pore as the potential from two walls placed at $y = \pm h$. The diffusion cross-section [Eq. (3)] is then

$$\sigma = 2w \int_0^h e^{-U(y)/(k_B T)} dy, \tag{A7a}$$

with $U(y) = q\psi(y)$ and

$$\psi(y) = 2\frac{k_B T}{Z_{el}e} \ln\left[\frac{1 + \tanh\left(\frac{Z_{el}e\zeta}{4k_B T} \right) e^{-(h-y)/\lambda_D}}{1 - \tanh\left(\frac{Z_{el}e\zeta}{4k_B T} \right) e^{-(h-y)/\lambda_D}} \right]. \tag{A7b}$$

Note Eq. (A7b) is a solution to the nonlinear Poisson-Boltzmann equation [31]. Carrying out the integral in Eq. (A7a) and taking the limit of $\sigma - \sigma_0$ for $h \to \infty$, we find the offset as

$$\Delta h = 4\lambda_D \sum_{k=1}^{N} \frac{1}{2(N-k)+1}\left[e^{-\frac{Z_{el}e\zeta}{k_B T}(N-k+1/2)} - 1 \right], \tag{A8}$$

when the ratio of the valence of the tracer particle to the ions in the electrolyte $N = |Z/Z_{el}|$ is an integer. An example illustrating Eq. (A6) is seen in Fig. 7.

The offset can also be found in the more general case where the potential at the two walls are not the same and the size of the particle is taken into account. If ϵ is the ratio of the value of the potential at the walls, ζ is the potential at one of the walls and d is the diameter of the tracer particles, the offset is

$$\Delta h = -d - 2\lambda_D \sum_{k=1}^{N} \frac{1}{2(N-k)+1} \left(2 + \left\{ \frac{\tanh[\text{sgn}(Z)Z_{el}e\zeta/(4k_B T)]e^{-d/(2\lambda_D)} - 1}{\tanh[\text{sgn}(Z)Z_{el}e\zeta/(4k_B T)]e^{-d/(2\lambda_D)} + 1} \right\}^{2(N-k)+1} \right.$$

$$\left. + \left\{ \frac{\tanh[\epsilon\,\text{sgn}(Z)Z_{el}e\zeta/(4k_B T)]e^{-d/(2\lambda_D)} - 1}{\tanh[\epsilon\,\text{sgn}(Z)Z_{el}e\zeta/(4k_B T)]e^{-d/(2\lambda_D)} + 1} \right\}^{2(N-k)+1} \right), \tag{A9}$$
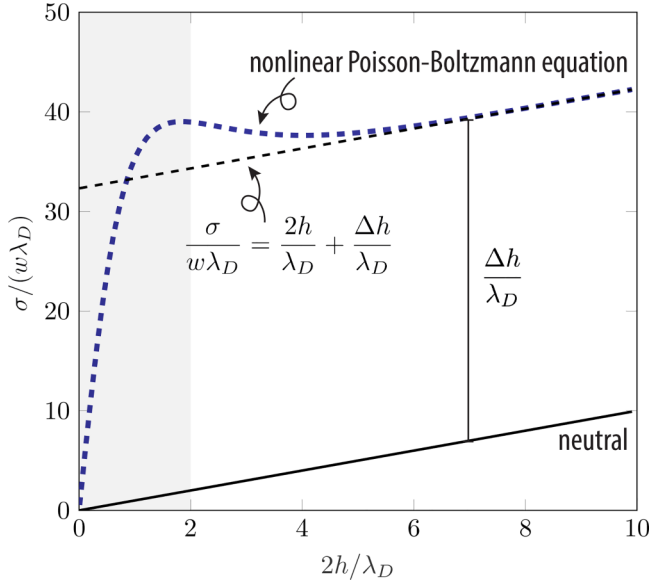
FIG. 7. Offset in the slit geometry. When the gap between the parallel plates is much larger than the Debye length, $2h \gg \lambda_D$, the diffusion cross-section increases linearly with channel height, $2h$, but with an offset Δh (thin dashed line). Here with energy scale $U_0/(k_B T) = -4$, tracer particle valence $Z = 2$ and surface potential $\zeta = -52$ mV. The dashed blue line is the diffusion cross-section found using the electric potential from the nonlinear Poisson-Boltzmann equation. The thin solid line corresponds to the interaction-free case $\sigma = \sigma_0 = 2hw$.

where sgn(Z) denotes the sign of Z.

We now look at channels with a circular cross-section and radius a in the limit of strongly nonoverlapping electric double layers, $a/\lambda_D \gg 1$. As the radius a of the channel approaches infinity, the curvature becomes negligible and the electric potential in the channel is approximately the potential from a single wall. The offset is thus the extra area gained from one wall, with a width corresponding to the circumference of the circular channel, $w = 2\pi a$. That is, we can write the diffusion cross-section as

$$\sigma = \sigma_0 + 2\pi a \frac{\Delta h}{2}, \qquad (A10)$$

with $\sigma_0 = \pi a^2$ and Δh from Eq. (A8).

4. Multipolar interaction energies

In this Appendix we show that neither pure multipolar interactions, nor potentials of the form $U = U_0 f(y/\ell)$, where f is a nondimensional function, can lead to local optima in the diffusion cross-section. In order for a local extrema to exist, the diffusion cross-section [Eq. (3)] must be a solution to Eq. (4).

We start by considering pure multipolar interactions. The interaction energy for pure multipolar interactions is on the form

$$U_{\mathrm{MP}}(y) = U_0 \frac{(2s)^n}{(h + 2s - y)^n}. \qquad (A11a)$$

The parameter n describes the type of interaction: $n = 1$ is ion-ion interactions, $n = 2$ is ion-dipole interactions, $n = 3$ is dipole-dipole interactions, and $n = 6$ is London type interac-

tions [38]. s is the radius or separation distance of the ions or dipoles, respectively.

If we let $\tilde{y} = h + 2s - y$, then the diffusion cross-section [Eq. (3)] is

$$\sigma_{\mathrm{MP}} = 2w \int_{2s}^{h+2s} \exp\left[-\frac{U_0}{k_B T} \left(\frac{2s}{\tilde{y}} \right)^n \right] d\tilde{y}. \qquad (A11b)$$

Differentiating with respect to channel height h,

$$\frac{d\sigma_{\mathrm{MP}}}{dh} = 2w \exp\left[-\frac{U_0}{k_B T} \left(\frac{2s}{h + 2s} \right)^n \right] > 0. \qquad (A11c)$$

As the derivative of σ_{MP} with respect to h is never zero, no local extrema exists for pure multipolar interactions.

Next, we look at interaction energies of the form

$$U(y) = U_0 f[y/(\ell/2)], \qquad (A12a)$$

where f is a nondimensional function and with no additional length scale apart from the channel size ℓ. First, for the slit geometry with $\ell = 2h$, let $\tilde{y} = y/h$. The diffusion cross-section is then

$$\sigma = 2wh \int_0^1 e^{-U_0 f(\tilde{y})/(k_B T)} d\tilde{y}. \qquad (A12b)$$

Differentiating with respect to channel height h,

$$\frac{d\sigma}{dh} = 2w \int_0^1 e^{-U_0 f(\tilde{y})/(k_B T)} d\tilde{y} = \mathrm{constant}. \qquad (A12c)$$

As the derivative is never zero, no local optima exists.

Lastly, if we now consider a cylindrical pore with a circular geometry, and let $\ell = 2a$, the interaction energy is on the form $U(r) = U_0 f(r/a)$ and the diffusion cross-section becomes

$$\sigma = 2\pi a^2 \int_0^1 e^{-U_0 f(\tilde{r})/(k_B T)} \tilde{r} d\tilde{r}, \qquad (A12d)$$

with $\tilde{r} = r/a$. Differentiating with respect to channel radius a,

$$\frac{d\sigma}{da} = 4\pi a \int_0^1 e^{-U_0 f(\tilde{r})/(k_B T)} \tilde{r} d\tilde{r} > 0, \qquad (A12e)$$

and as the derivative is never zero, no local optima exists here either.

5. Validity of the Debye-Hückel approximation

Up until now, we have used the Debye-Hückel approximation to find the energy potential through which the tracer particles interact with the channel boundaries, when the channel surfaces are charged (with surface potential ζ) and the channel contains an electrolyte solution. In this section, we discuss the validity of this approximation. The interaction potential for a tracer particle with charge $q = Ze$, where Z is the tracer particle valence, interacting with the electrical double layer in the channel is the product of the tracer particle charge and the electric potential ψ in the channel, $U = q\psi$. To find the electric potential in the channel, we have so far used the Debye-Hückel approximation, i.e., the linearized Poisson-Boltzmann equation.

In general, the electric potential found from a charged surface in contact with an electrolyte solution can be described by the Poisson-Boltzmann equation [31]. For a symmetric electrolyte, i.e., when the ions in the electrolyte have valences

$\pm Z_{\text{el}}$, the nonlinear Poisson-Boltzmann equation is

$$\nabla^2 \psi = \frac{2c_{\text{el}} Z_{\text{el}} e}{\varepsilon} \sinh\left(\frac{Z_{\text{el}} e \psi}{k_B T}\right). \tag{A13}$$

Analytical solutions to this equation, however, only exist for very few geometries, and not for the ones we consider here. The Debye-Hückel approximation, a linearization of the Poisson-Boltzmann equation valid in the limit when the ratio of the electrical to thermal potential is small, $|\psi e Z_{\text{el}}/(k_B T)| \ll 1$, can be used to provide analytical solutions of the electric potential in this limit. Instead of solving the nonlinear Poisson-Boltzmann equation, one solves the linearized Poisson-Boltzmann equation

$$\nabla^2 \psi = \frac{1}{\lambda_D^2} \psi, \tag{A14}$$

where $\lambda_D = \sqrt{\varepsilon k_B T / (2(Z_{\text{el}} e)^2 c_{\text{el}})}$ is the Debye length. When finding the electric potential in the channels, we use the boundary conditions that the potentials at the channel surfaces are given. We note that the electric potential in the channel being low, $|\psi e Z_{\text{el}}/(k_B T)| \leqslant |\zeta e Z_{\text{el}}/(k_B T)| \ll 1$, does not necessarily mean that the energy scale $U_0/(k_B T) = Z e \zeta /(k_B T)$ is small. The energy scale U_0 also depends on the tracer particle valence Z. The linearized Poisson-Boltzmann equation can thus still be used in the interaction energy to find the diffusion cross-section when U_0 is not small, if the channel surface potential, ζ, is small and the tracer particle valence, Z, is large instead.

If we move beyond the validity of the linearized Poisson-Boltzmann equation, then we can find the diffusion cross-section using the numerical solution of the nonlinear Poisson-Boltzmann equation instead to find the electric potential in the interaction energy. When the electrical potential is found numerically from the nonlinear Poisson-Boltzmann equation, we still see the same types of behaviours as observed when the linearized Poisson-Boltzmann equation is used. In particular, we still find the local extrema in the diffusion cross-section in the parallel plate geometry (Fig. 8). The absolute value of the diffusion cross-section may, however, be different when the electric potential in the interaction energy is found numerically from the nonlinear Poisson-Boltzmann equation compared to when it is found using the linearized Poisson-Boltzmann equation.

For example, for a relative interaction energy of $U_0/(k_B T) = -4$, electrolyte valence $Z_{\text{el}} = 1$, and temperature $T = 300$ K, the relative deviation of the value of the diffusion cross-section $\sigma/(w\lambda_D)$ at the local optimum varies from approximately 16% for tracer particle valence and surface potential $Z = 2$ and $\zeta = -52$ mV [Fig. 8(a)] to approximately 2.2% for tracer particle valence and surface potential $Z = 6$ and $\zeta = -17$ mV [Fig. 8(d)]. For a tracer particle valence and surface potential $Z = 3$ and $\zeta = -34$ mV, the relative deviation is $\sim$8.1% [Fig. 8(b)] and for $Z = 4$ and $\zeta = -26$ mV it is $\sim$4.8% [Fig. 8(c)].

Last, we note that when the linearized Poisson-Boltzmann equation is used, the dependence on the channel surface potential, ζ, and tracer particle valence, Z, is solely through their product in the energy scale U_0. However, this is not so when the potential is found numerically from the nonlinear Poisson-Boltzmann equation, and the value of the energy scale, U_0, at
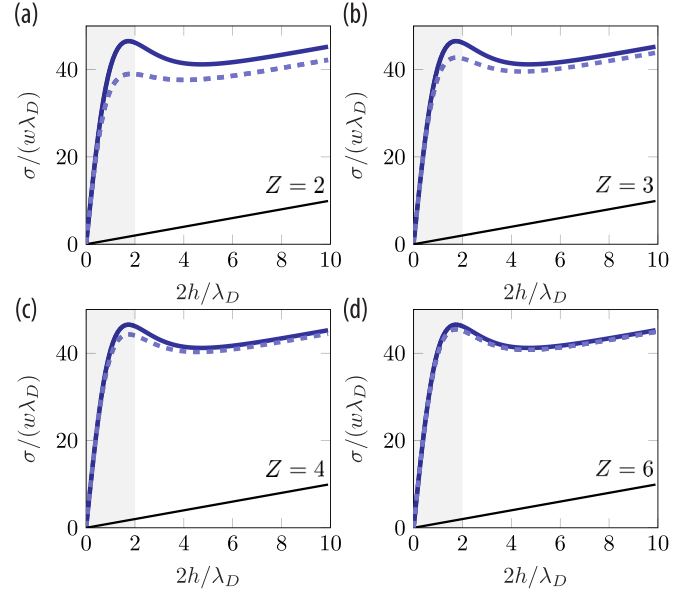

FIG. 8. Surface-enhanced diffusion in a slit. A local maximum in the diffusion cross-section σ as a function of channel height $2h$ also exists when the electric potential in the slit is found by solving the nonlinear Poisson-Boltzmann equation numerically (dashed blue lines). Here shown for relative interaction energy $U_0/(k_B T) = -4$ and electrolyte valence $Z_{\text{el}} = 1$. (a) Tracer particle valence $Z = 2$ and surface potential $\zeta = -52$ mV. (b) Tracer particle valence $Z = 3$ and surface potential $\zeta = -34$ mV. (c) Tracer particle valence $Z = 4$ and surface potential $\zeta = -26$ mV. (d) Tracer particle valence $Z = 6$ and surface potential $\zeta = -17$ mV. The solid blue line shows the corresponding diffusion cross-section when the electric potential in the channel is found using the linearized Poisson-Boltzmann equation for $U_0/(k_B T) = -4$. The thin solid line corresponds to the interaction-free case $\sigma = \sigma_0$. Note that when the electric potential, and hence interaction energy $U(y)$, is found by solving the nonlinear Poisson-Boltzmann equation numerically, the diffusion cross-section depends on the tracer particle valence, Z, and channel surface potential, ζ, separately and not only on their product as seen when the Debye-Hückel approximation is used.

which the local extrema appear can differ from the one found when the linearized Poisson-Boltzmann equation is used.

6. Flux of tracer particles from the Nernst-Planck equation

In the following Appendix, we compare the terms in the tracer particle flux from the Nernst-Planck equation, to see that the diffusive flux term is the dominating one. We do this when the parameter $\alpha = \frac{c_0}{c_{\text{el}}} \frac{Z^2}{Z_{\text{el}}^2} \ll 1$, which is the ratio of the interaction-free concentration and valence squared of the tracer particles to the electrolyte ions, is small.

We consider the parallel plate geometry, with channel length L in the z direction and height $2h$ in the y direction. The channel is assumed to be long and slender, so $2h/L \ll 1$. There are four ion species in the solution: the positive and negative ions from the electrolyte with concentrations $c_{\text{el},\pm}$ and valences $Z_{\text{el},+} = -Z_{\text{el},-} = Z_{\text{el}}$, and the positively and negatively charged tracer particles with concentrations $c_\pm$ and valences $Z_+ = -Z_- = Z$. The concentration of the electrolyte ions do not vary with z and $c_{\text{el},\pm}(z=0) = c_{\text{el},\pm}(z=L) = c_{\text{el}}$.

There is, however, a difference in tracer particle concentration across the channel, with $c_\pm(z=0) = \Delta c$ and $c_\pm(z=L) = 0$. Further, we assume the concentration of tracer particles is much smaller than that of the electrolyte $c \ll c_{\rm el}$.

The governing equations are

$$\mathbf{J}_i = -D_i \nabla c_i + \mathbf{u}c_i - \frac{D_i Z_i e c_i}{k_B T} \nabla \phi, \qquad (\text{A15a})$$

$$\nabla \cdot \mathbf{J}_i = 0, \qquad (\text{A15b})$$

$$\nabla^2 \phi = -\frac{\rho_e}{\varepsilon} = -\frac{e}{\varepsilon} \sum_i Z_i c_i, \qquad (\text{A15c})$$

$$\nabla \cdot \mathbf{u} = 0, \qquad (\text{A15d})$$

$$\eta \nabla^2 \mathbf{u} = \nabla p + \rho_e \nabla \phi, \qquad (\text{A15e})$$

with $\mathbf{J}_i = J_{iz}\mathbf{e}_z + J_{iy}\mathbf{e}_y$, c_i, D_i, and Z_i, the flux, concentration, diffusivity, and valence of the ith ion, respectively, $\rho_e = e \sum_i Z_i c_i$ the charge density, $\phi(y,z)$ the electric potential, $\mathbf{u} = u_z\mathbf{e}_z + u_y\mathbf{e}_y$ the velocity field, p the pressure, and η the viscosity [39]. We assume the velocity is zero at the walls, i.e., $\mathbf{u}(y=\pm h, z) = \mathbf{0}$.

To justify Eq. (1), we want to evaluate the magnitude of the terms in the z component of Eq. (A15a) for the positively charged tracer particle. Our main finding is that the flux of positive tracer particles can be written as

$$J_{+z} = -D_+ e^{-\frac{Ze\psi_0}{k_B T}} \frac{\partial c_0}{\partial z} + O(\alpha), \qquad (\text{A16})$$

where ψ_0 is the electric potential in a channel containing only the electrolyte ions (i.e., no tracer particles), c_0 is the concentration of tracer particles in an uncharged channel, and $\alpha = \frac{c_0}{c_{\rm el}}\frac{Z^2}{Z_{\rm el}^2}$. With $\alpha = \frac{c_0}{c_{\rm el}}\frac{Z^2}{Z_{\rm el}^2} \ll 1$ the diffusive part of the flux dominates and the use of pure diffusive transport in Eq. (1) is justified.

Proceeding with the detailed calculations, we first need to find the velocity u_z and the gradient of the potential $\frac{\partial \phi}{\partial z}$. The normal fluxes at the boundaries should vanish, that is, $J_{iy}(z, y=\pm h) = 0$, from which the concentration of the ith ion is

$$c_i(y,z) = c_{i0}(z) e^{-Z_i e \psi(y,z)/(k_B T)}. \qquad (\text{A17})$$

Here, we let the electric potential $\phi(y,z) = \psi(y,z) + \psi_*(z)$, and define $c_{i0}(z)$ and $\psi_*(z)$ as the concentration of the ith ion and the potential in the channel when the surface potential $\zeta = 0$. For the bulk electrolyte ions the concentration, $c_{{\rm el},\pm 0}(z) = c_{\rm el}$, is independent of z.

Next, we look at Eq. (A15c) and insert the concentrations from Eq. (A17). First, as the channel length is much larger than its height, $2h/L \ll 1$, $\nabla^2 \approx \frac{\partial^2}{\partial y^2}$, and

$$\frac{\partial^2 \phi}{\partial y^2} = \frac{\partial^2 \psi}{\partial y^2} = -\frac{e}{\varepsilon}[Z_{\rm el}(c_{{\rm el},+} - c_{{\rm el},-}) + Z(c_+ - c_-)]$$

$$= \frac{2Z_{\rm el} e c_{\rm el}}{\varepsilon} \sinh\left(\frac{Z_{\rm el} e \psi}{k_B T}\right)$$

$$\times \left[1 + \frac{Z}{Z_{\rm el}}\frac{c_0(z)}{c_{\rm el}}\frac{\sinh\left(\frac{Ze\psi}{k_B T}\right)}{\sinh\left(\frac{Z_{\rm el} e \psi}{k_B T}\right)}\right]$$

$$\simeq \frac{1}{\lambda_D^2}\psi\left[1 + \delta(z)\left(\frac{Z}{Z_{\rm el}}\right)^2\right], \qquad (\text{A18a})$$

where $\delta(z) = c_0(z)/c_{\rm el} \ll 1$, and the Debye length $\lambda_D = \sqrt{\varepsilon k_B T/[2c_{\rm el}(Z_{\rm el}e)^2]}$. In the last step, we have used the Debye-Hückel approximation assuming $|Z_{\rm el}e\psi/(k_B T)| < 1$. Letting $\alpha(z) = \delta(z)(Z/Z_{\rm el})^2$, we can write the Poisson-Boltzmann equation in the Debye-Hückel limit as

$$\frac{\partial^2 \psi}{\partial y^2} \simeq \frac{1}{\lambda_D^2}\psi[1 + \alpha(z)]. \qquad (\text{A18b})$$

The potential ψ is then found using the boundary conditions that the potential is constant at the channel surface, $\psi(y=\pm h, z) = \zeta$, as

$$\psi(y,z) = \zeta \frac{\cosh\left(\frac{y\sqrt{1+\alpha(z)}}{\lambda_D}\right)}{\cosh\left(\frac{h\sqrt{1+\alpha(z)}}{\lambda_D}\right)}. \qquad (\text{A18c})$$

To find the axial velocity u_z we first need the pressure p. From the y component of Eq. (A15e) (assuming the $\eta\nabla^2 u_y$ term is small)

$$\frac{\partial p}{\partial y} = -\rho_e \frac{\partial \psi}{\partial y} \simeq \frac{\varepsilon}{\lambda_D^2}(1+\alpha(z))\psi\frac{\partial \psi}{\partial y}. \qquad (\text{A19a})$$

Integrating once we find the pressure as

$$p(y,z) = \frac{\varepsilon}{2\lambda_D^2}(1+\alpha(z))\psi^2(y,z) + p_0(z), \qquad (\text{A19b})$$

where $p_0(z)$ is the pressure in the channel when the potential at the channel surface is zero ($\psi(y=\pm h) = \zeta = 0$).

Having found the pressure, we look at the z component of Eq. (A15e) to find the velocity. As the channel length is much larger than its height, $2h/L \ll 1$, we again have $\nabla^2 \simeq \frac{\partial^2}{\partial y^2}$, and

$$\eta\frac{\partial^2 u_z}{\partial y^2} \simeq \frac{\partial p}{\partial z} + \rho_e\left(\frac{\partial \psi}{\partial z} + \frac{\partial \psi_*}{\partial z}\right)$$

$$= \frac{\partial p_0(z)}{\partial z} + \frac{\partial \alpha(z)}{\partial z}\frac{\varepsilon}{2\lambda_D^2}\psi^2 - \varepsilon\frac{\partial \psi_*(z)}{\partial z}\frac{\partial^2 \psi}{\partial y^2}. \qquad (\text{A20a})$$

Integrating twice and using the no-slip boundary conditions $[u_z(y=\pm h) = 0]$,

$$u_z(y,z) = \frac{1}{2\eta}\frac{\partial p_0}{\partial z}(y^2 - h^2) + \frac{\varepsilon}{\eta}\frac{\partial \psi_*}{\partial z}(\zeta - \psi)$$

$$+ \frac{\partial \alpha(z)}{\partial z}\frac{\varepsilon}{8\eta}\left\{\frac{\psi^2 - \zeta^2}{1+\alpha(z)}\right.$$

$$\left. + \frac{\zeta^2}{\lambda_D^2}\frac{y^2 - h^2}{\cosh[h\sqrt{1+\alpha(z)}/\lambda_D]}\right\}. \qquad (\text{A20b})$$

To find the potential $\frac{\partial \psi_*}{\partial z}$ we use the zero current condition, i.e.,

$$\tilde{I} = \int_{-h}^{h} \left(\sum_i Z_i J_{iz} \right) dy = 0 \tag{A21a}$$

$$= \tilde{I}_d + \tilde{I}_s + \tilde{I}_c, \tag{A21b}$$

with

$$\tilde{I}_d = \int_{-h}^{h} i_d dy, \tag{A22a}$$

$$\tilde{I}_s = \int_{-h}^{h} i_s dy, \tag{A22b}$$

$$\tilde{I}_c = \int_{-h}^{h} i_c dy, \tag{A22c}$$

and

$$i_d = -\sum_i Z_i D_i \frac{\partial c_i}{\partial z}$$

$$\simeq -Z(D_+ - D_-) \frac{\partial c_0}{\partial z} \left(1 - \frac{D_+ + D_-}{D_+ - D_-} \frac{Ze\psi}{k_B T} \right) + \frac{\varepsilon}{2\lambda_D^2 e} \frac{\partial \psi}{\partial z} (D_{\text{el},+} + D_{\text{el},-}) \left(1 + \alpha(z) \frac{D_+ + D_-}{D_{\text{el},+} + D_{\text{el},-}} \right), \tag{A23a}$$

$$i_s = \sum_i Z_i c_i u_z = -u_z \frac{\varepsilon}{e} \frac{\partial^2 \psi}{\partial y^2}$$

$$\simeq -\frac{\varepsilon}{e} \frac{\partial^2 \psi}{\partial y^2} \left[\frac{1}{2\eta} \frac{\partial p_0}{\partial z} (y^2 - h^2) + \frac{\varepsilon}{\eta} \frac{\partial \psi_*}{\partial z} (\zeta - \psi) + \frac{\partial \alpha(z)}{\partial z} \frac{\varepsilon}{8\eta} \left(\frac{\psi^2 - \zeta^2}{1 + \alpha(z)} + \frac{\zeta^2}{\lambda_D^2} \frac{y^2 - h^2}{\cosh(h\sqrt{1 + \alpha(z)}/\lambda_D)} \right) \right], \tag{A23b}$$

$$i_c = -\sum_i \frac{D_i(Z_i)^2 e c_i}{k_B T} \frac{\partial \phi}{\partial z}$$

$$\simeq -\left(\frac{\partial \psi_*}{\partial z} + \frac{\partial \psi}{\partial z} \right) \frac{\varepsilon}{2\lambda_D^2 e} (D_{\text{el},+} + D_{\text{el},-}) \left[1 - \frac{D_{\text{el},+} - D_{\text{el},-}}{D_{\text{el},+} + D_{\text{el},-}} \frac{Z_{\text{el}} e \psi}{k_B T} + \alpha(z) \left(\frac{D_+ + D_-}{D_{\text{el},+} + D_{\text{el},-}} - \frac{Ze\psi}{k_B T} \frac{D_+ - D_-}{D_{\text{el},+} + D_{\text{el},-}} \right) \right]. \tag{A23c}$$

Here, the Debye-Hückel approximation is used to expand the concentrations around $Z_{\text{el}} e\psi / (k_B T)$.

The currents are then

$$\tilde{I}_d \simeq -Z\tilde{D}^{(-)} \frac{\partial c_0}{\partial z} \left(2h - \frac{\tilde{D}^{(+)}}{\tilde{D}^{(-)}} \frac{Ze}{k_B T} \int_{-h}^{h} \psi dy \right) + \frac{\varepsilon}{2\lambda_D^2 e} \tilde{D}_{\text{el}}^{(+)} \left(1 + \alpha(z) \frac{\tilde{D}^{(+)}}{\tilde{D}_{\text{el}}^{(+)}} \right) \int_{-h}^{h} \frac{\partial \psi}{\partial z} dy, \tag{A24a}$$

$$\tilde{I}_s \simeq -\frac{\partial \psi_*}{\partial z} \frac{\varepsilon^2}{\eta e} \int_{-h}^{h} \left(\frac{\partial \psi}{\partial y} \right)^2 dy + \frac{\varepsilon}{\eta e} \frac{\partial p_0}{\partial z} \left(2h\zeta - \int_{-h}^{h} \psi dy \right) + \frac{\partial \alpha(z)}{\partial z} \frac{\varepsilon^2}{4\eta e(1 + \alpha(z))} \int_{-h}^{h} \psi \left(\frac{\partial \psi}{\partial y} \right)^2 dy, \tag{A24b}$$

$$\tilde{I}_c \simeq -\frac{\partial \psi_*}{\partial z} \frac{\varepsilon}{2\lambda_D^2 e} \tilde{D}_{\text{el}}^{(+)} \left[2h - \frac{\tilde{D}_{\text{el}}^{(-)}}{\tilde{D}_{\text{el}}^{(+)}} \frac{Z_{\text{el}} e}{k_B T} \int_{-h}^{h} \psi dy + \alpha(z) \left(\frac{\tilde{D}^{(+)}}{\tilde{D}_{\text{el}}^{(+)}} 2h - \frac{\tilde{D}^{(-)}}{\tilde{D}_{\text{el}}^{(+)}} \frac{Ze}{k_B T} \int_{-h}^{h} \psi dy \right) \right]$$

$$- \frac{\varepsilon}{2\lambda_D^2 e} \tilde{D}_{\text{el}}^{(+)} \left[\int_{-h}^{h} \frac{\partial \psi}{\partial z} dy - \frac{\tilde{D}_{\text{el}}^{(-)}}{\tilde{D}_{\text{el}}^{(+)}} \frac{Z_{\text{el}} e}{k_B T} \int_{-h}^{h} \psi \frac{\partial \psi}{\partial z} dy + \alpha(z) \left(\frac{\tilde{D}^{(+)}}{\tilde{D}_{\text{el}}^{(+)}} \int_{-h}^{h} \frac{\partial \psi}{\partial z} dy - \frac{\tilde{D}^{(-)}}{\tilde{D}_{\text{el}}^{(+)}} \frac{Ze}{k_B T} \int_{-h}^{h} \psi \frac{\partial \psi}{\partial z} dy \right) \right], \tag{A24c}$$

where we have introduced $\tilde{D}^{(+)} = D_+ + D_-$, $\tilde{D}^{(-)} = D_+ - D_-$, $\tilde{D}_{\mathrm{el}}^{(+)} = D_{\mathrm{el},+} + D_{\mathrm{el},-}$ and $\tilde{D}_{\mathrm{el}}^{(-)} = D_{\mathrm{el},+} - D_{\mathrm{el},-}$. Last, we find the potential $\frac{\partial \psi_*}{\partial z}$ from $\tilde{I}_d + \tilde{I}_s + \tilde{I}_c = 0$ (for $\frac{\partial p_0}{\partial z} = 0$) as

$$
\begin{aligned}
\frac{\partial \psi_*}{\partial z} &= \frac{-Z\tilde{D}^{(-)}\frac{\partial c_0}{\partial z}\left(2h - \frac{\tilde{D}^{(+)}}{\tilde{D}^{(-)}}\frac{Ze}{k_BT}\int_{-h}^{h}\psi\,dy\right) + \frac{\partial \alpha(z)}{\partial z}\frac{\varepsilon^2}{4\eta e(1+\alpha(z))}\int_{-h}^{h}\psi\left(\frac{\partial\psi}{\partial y}\right)^2 dy + \frac{\varepsilon\tilde{D}_{\mathrm{el}}^{(-)}}{2\lambda_D^2 e}\frac{Z_{\mathrm{el}}e}{k_BT}\left(1+\alpha(z)\frac{Z}{Z_{\mathrm{el}}}\frac{\tilde{D}^{(-)}}{\tilde{D}_{\mathrm{el}}^{(-)}}\right)\int_{-h}^{h}\psi\frac{\partial\psi}{\partial z}\,dy}{-\frac{\varepsilon^2}{\eta e}\int_{-h}^{h}\left(\frac{\partial\psi}{\partial y}\right)^2 dy - \frac{\varepsilon\tilde{D}_{\mathrm{el}}^{(+)}}{2\lambda_D^2 e}\left[2h\left(1+\alpha(z)\frac{\tilde{D}^{(+)}}{\tilde{D}_{\mathrm{el}}^{(+)}}\right) - \frac{Z_{\mathrm{el}}e}{k_BT}\frac{\tilde{D}_{\mathrm{el}}^{(-)}}{\tilde{D}_{\mathrm{el}}^{(+)}}\left(1+\alpha(z)\frac{Z}{Z_{\mathrm{el}}}\frac{\tilde{D}^{(-)}}{\tilde{D}_{\mathrm{el}}^{(-)}}\right)\int_{-h}^{h}\psi\,dy\right]} \\[2mm]
&= \frac{\frac{1}{c_{\mathrm{el}}}\frac{Z^2}{Z_{\mathrm{el}}^2}\frac{k_BT}{Ze}\frac{\tilde{D}^{(-)}}{\tilde{D}_{\mathrm{el}}^{(+)}}\frac{\partial c_0}{\partial z}\left(1 - \frac{\tilde{D}^{(+)}}{\tilde{D}^{(-)}}\frac{Ze}{k_BT}\frac{1}{2h}\int_{-h}^{h}\psi\,dy\right) - \frac{\tilde{D}_{\mathrm{el}}^{(-)}}{\tilde{D}_{\mathrm{el}}^{(+)}}\frac{Z_{\mathrm{el}}e}{k_BT}\frac{1}{2h}\int_{-h}^{h}\psi\frac{\partial\psi}{\partial z}\,dy\left(1+\alpha\frac{Z}{Z_{\mathrm{el}}}\frac{\tilde{D}^{(-)}}{\tilde{D}_{\mathrm{el}}^{(-)}}\right) - \frac{\partial\alpha}{\partial z}\frac{\varepsilon\lambda_D^2}{2\eta\tilde{D}_{\mathrm{el}}^{(+)}}\frac{1}{1+\alpha}\frac{1}{2h}\int_{-h}^{h}\psi\left(\frac{\partial\psi}{\partial y}\right)^2 dy}{1 + \frac{\tilde{D}_{\mathrm{el}}^{(-)}}{\tilde{D}_{\mathrm{el}}^{(+)}}\frac{Z_{\mathrm{el}}e}{k_BT}\frac{1}{2h}\int_{-h}^{h}\psi\,dy + \frac{2\lambda_D^2\varepsilon}{\eta\tilde{D}_{\mathrm{el}}^{(+)}}\frac{1}{2h}\int_{-h}^{h}\left(\frac{\partial\psi}{\partial y}\right)^2 dy + \alpha\frac{\tilde{D}^{(+)}}{\tilde{D}_{\mathrm{el}}^{(+)}}\left(1 + \frac{Z}{Z_{\mathrm{el}}}\frac{Z_{\mathrm{el}}e}{k_BT}\frac{1}{2h}\int_{-h}^{h}\psi\,dy\right)}.
\end{aligned}
$$
$$\tag{A25}$$

Comparing the terms in the tracer particle flux

Having found the velocity u_z and the gradient of the potential $\frac{\partial \psi_*}{\partial z}$ we can now compare the magnitude of the different terms in the tracer particle flux. The flux of positive tracer particles in the z direction is, from Eq. (A15a),

$$
J_{+z} = -D_+\frac{\partial c_+}{\partial z} + u_z c_+ - \frac{D_+ Zec_+}{k_BT}\frac{\partial\phi}{\partial z}. \tag{A26}
$$

To compare the magnitude of the different terms, when the concentration of the tracer particles is much smaller than the concentration of electrolyte ions, i.e., $\alpha = \frac{c_0}{c_{\mathrm{el}}}\frac{Z^2}{Z_{\mathrm{el}}^2} \ll 1$, we consider each term individually. First, however, we note that the potential in the channel ψ [Eq. (A18c)] can be written as $\psi(y,z) \simeq \psi_0(y) + \alpha(z)\psi_1(y) + O(\alpha^2)$ for small α, where $\psi_0(y)$ and $\psi_1(y)$ are functions of y only and not of z. From this we see $\frac{\partial\psi}{\partial z} \simeq \frac{\partial\alpha}{\partial z}\psi_1(y)$. And last, from the definition of $\alpha(z) = \frac{c_0(z)}{c_{\mathrm{el}}}\frac{Z^2}{Z_{\mathrm{el}}^2}$, we also note $c_0(z)\frac{\partial\alpha(z)}{\partial z} = \alpha(z)\frac{\partial c_0(z)}{\partial z}$.

Now, looking at the individual terms, the diffusive term in the flux [Eq. (A26)] is

$$
D_+\frac{\partial c_+}{\partial z} = -D_+ e^{-\frac{Ze\psi_0}{k_BT}}\frac{\partial c_0}{\partial z}\left(1 - \alpha\frac{2Ze\psi_1}{k_BT}\right) + O(\alpha^2) = -D_+ e^{-\frac{Ze\psi_0}{k_BT}}\frac{\partial c_0}{\partial z} + O(\alpha). \tag{A27a}
$$

The second term in the flux [Eq. (A26)] is

$$
u_z c_+ = u_z c_0 e^{-\frac{Ze\psi_0}{k_BT}}\left(1 - \alpha\frac{Ze\psi_1}{k_BT}\right) + O(\alpha^2) = O(\alpha), \tag{A27b}
$$

where the second equality comes from $c_0 u_z = O(\alpha)$ [Eqs. (A20b) and (A25)].

And the last term in the flux [Eq. (A26)] is

$$
-\frac{D_+ Zec_+}{k_BT}\frac{\partial\phi}{\partial z} = -\frac{D_+ Ze}{k_BT}e^{-\frac{Ze\psi_0}{k_BT}}\left(1 - \alpha\frac{Ze\psi_1}{k_BT}\right)\left(\alpha\psi_1\frac{\partial c_0}{\partial z} + c_0\frac{\partial\psi_*}{\partial z}\right) + O(\alpha^2) = O(\alpha), \tag{A27c}
$$

where the second equality comes from $c_0\frac{\partial\psi_*}{\partial z} = O(\alpha)$ [Eq. (A25)].

The positive tracer particle flux [Eq. (A26)] is therefore

$$
J_{+z} = -D_+ e^{-\frac{Ze\psi_0}{k_BT}}\frac{\partial c_0}{\partial z} + O(\alpha), \tag{A28}
$$

and we see that the diffusive part of the flux dominates.

[1] L. Wang, M. S. Boutilier, P. R. Kidambi, D. Jang, N. G. Hadjiconstantinou, and R. Karnik, Fundamental transport mechanisms, fabrication, and potential applications of nanoporous atomically thin membranes, Nat. Nanotechnol. **12**, 509 (2017).

[2] D. S. Sholl and R. P. Lively, Seven chemical separations to change the world, Nature (London) **532**, 435 (2016).

[3] Z. Wang, L. Wang, and M. Elimelech, Viability of harvesting salinity gradient (blue) energy by nanopore-based osmotic power generation, Engineering **9**, 51 (2022).

[4] L. Cao, Q. Wen, Y. Feng, D. Ji, H. Li, N. Li, L. Jiang, and W. Guo, On the origin of ion selectivity in ultrathin nanopores: Insights for membrane-scale osmotic energy conversion, Adv. Funct. Mater. **28**, 1804189 (2018).

[5] G. S. Goldberg, V. Valiunas, and P. R. Brink, Selective permeability of gap junction channels, Biochim. Biophys. Acta, Biomembr. **1662**, 96 (2004).

[6] S. Gravelle, L. Joly, F. Detcheverry, C. Ybert, C. Cottin-Bizonne, and L. Bocquet, Optimizing water permeability through the hourglass shape of aquaporins, Proc. Natl. Acad. Sci. USA **110**, 16367 (2013).

[7] C. Zhang and S. Scholpp, Cytonemes in development, Curr. Opin. Genet. Dev. **57**, 25 (2019).

[8] W. S. Peters, K. H. Jensen, H. A. Stone, and M. Knoblauch, Plasmodesmata and the problems with size: Interpreting the confusion, J. Plant Physiology **257**, 153341 (2021).

[9] R. Koebnik, The role of bacterial pili in protein and DNA translocation, Trends Microbiol. **9**, 586 (2001).

[10] L. M. Robeson, The upper bound revisited, J. Membr. Sci. **320**, 390 (2008).

[11] L. Bocquet and E. Charlaix, Nanofluidics, from bulk to interfaces, Chem. Soc. Rev. **39**, 1073 (2010).

[12] A. Plecis, R. B. Schoch, and P. Renaud, Ionic transport phenomena in nanofluidics: Experimental and theoretical study of the exclusion-enrichment effect on a chip, Nano Lett. **5**, 1147 (2005).

[13] G. Bruno, N. Di Trani, R. L. Hood, E. Zabre, C. S. Filgueira, G. Canavese, P. Jain, Z. Smith, D. Demarchi, S. Hosali *et al.*, Unexpected behaviors in molecular transport through size-controlled nanochannels down to the ultra-nanoscale, Nat. Commun. **9**, 1682 (2018).

[14] S. Ghosal, Electrophoresis of a polyelectrolyte through a nanopore, Phys. Rev. E **74**, 041901 (2006).

[15] D. Stein, M. Kruithof, and C. Dekker, Surface-charge-governed ion transport in nanofluidic channels, Phys. Rev. Lett. **93**, 035901 (2004).

[16] S. Pennathur and J. G. Santiago, Electrokinetic transport in nanochannels. 1. Theory, Anal. Chem. **77**, 6772 (2005).

[17] S. Pennathur and J. G. Santiago, Electrokinetic transport in nanochannels. 2. Experiments, Anal. Chem. **77**, 6782 (2005).

[18] W. Deen, Hindered transport of large molecules in liquid-filled pores, AIChE J. **33**, 1409 (1987).

[19] A. J. Goldman, R. G. Cox, and H. Brenner, Slow viscous motion of a sphere parallel to a plane wall-I motion through a quiescent fluid, Chem. Eng. Sci. **22**, 637 (1967).

[20] R. Zando, M. Chinappi, C. Giordani, F. Cecconi, and Z. Zhang, Surface-particle interactions control the escape time of a particle from a nanopore-gated nanocavity system: A coarse-grained simulation, Nanoscale **15**, 11107 (2023).

[21] G. Oshanin, M. Tamm, and O. Vasilyev, Narrow-escape times for diffusion in microdomains with a particle-surface affinity: Mean-field results, J. Chem. Phys. **132**, 235101 (2010).

[22] K. Lin, Z. Li, Y. Tao, K. Li, H. Yang, J. Ma, T. Li, J. Sha, and Y. Chen, Surface charge density inside a silicon nitride nanopore, Langmuir **37**, 10521 (2021).

[23] P. Malgaretti, M. Janssen, I. Pagonabarraga, and J. M. Rubi, Driving an electrolyte through a corrugated nanopore, J. Chem. Phys. **151**, 084902 (2019).

[24] I. Rubinstein and B. Zaltzman, Convective diffusive mixing in concentration polarization: From Taylor dispersion to surface convection, J. Fluid Mech. **728**, 239 (2013).

[25] B. M. Alessio, S. Shim, A. Gupta, and H. A. Stone, Diffusioosmosis-driven dispersion of colloids: A Taylor dispersion analysis with experimental validation, J. Fluid Mech. **942**, A23 (2022).

[26] W. Sparreboom, A. van den Berg, and J. C. Eijkel, Principles and applications of nanofluidic transport, Nat. Nanotechnol. **4**, 713 (2009).

[27] R. K. Adair, Neutron cross sections of the elements, Rev. Mod. Phys. **22**, 249 (1950).

[28] H. C. Berg, *Random Walks in Biology* (Princeton University Press, Princeton, NJ, 1993).

[29] P. Debye and E. Hückel, The theory of electrolytes. I. Freezing point depression and related phenomena [translated by M. J. Braus (2020)], Phys. Z. **24**, 185 (1923).

[30] F. G. Smith III and W. M. Deen, Electrostatic effects on the partitioning of spherical colloids between dilute bulk solution and cylindrical pores, J. Colloid Interface Sci. **91**, 571 (1983).

[31] B. J. Kirby, *Micro- and Nanoscale Fluid Mechanics: Transport in Microfluidic Devices* (Cambridge University Press, Cambridge, UK, 2010).

[32] B. S. Der, C. Kluwe, A. E. Miklos, R. Jacak, S. Lyskov, J. J. Gray, G. Georgiou, A. D. Ellington, and B. Kuhlman, Alternative computational protocols for supercharging protein surfaces for reversible unfolding and retention of stability, PLoS One **8**, e64363 (2013).

[33] B. J. Kirby and E. F. Hasselbrink Jr., Zeta potential of microfluidic substrates: 1. Theory, experimental techniques, and effects on separations, Electrophoresis **25**, 187 (2004).

[34] T. B. Kinraide and P. Wang, The surface charge density of plant cell membranes (σ): An attempt to resolve conflicting values for intrinsic σ, J. Exp. Bot. **61**, 2507 (2010).

[35] D. W. Keizer, C. M. Slupsky, M. Kalisiak, A. P. Campbell, M. P. Crump, P. A. Sastry, B. Hazes, R. T. Irvin, and B. D. Sykes, Structure of a pilin monomer from *Pseudomonas aeruginosa*: Implications for the assembly of pili, J. Biol. Chem. **276**, 24186 (2001).

[36] H. Bruus, *Theoretical Microfluidics* (Oxford University Press, Oxford, UK, 2007), Vol. 18.

[37] D. J. Griffiths, *Introduction to Electrodynamics*, 4th ed. (Pearson Educational Limited, London, UK, 2014).

[38] P. Atkins and J. de Paula, *Atkins' Physical Chemistry*, 8th ed. (Oxford University Press, Oxford, UK, 2006).

[39] A. Gupta, B. Rallabandi, and H. A. Stone, Diffusiophoretic and diffusioosmotic velocities for mixtures of valence-asymmetric electrolytes, Phys. Rev. Fluids **4**, 043702 (2019).